DOI: 10.48011/asba.v2i1.1638

Modeling, Control and Regenerative Braking of BLDC Machines in Electric Bycicles ⋆

Elmer O. H. Catata * **Pedro J. dos Santos Neto** ** **Tárcio A. S. Barros** ** **Ernesto Ruppert Filho** **

* *Department of Electrical Engineering, Federal University of Acre, Brazil, (e-mail: elmerhc110@gmail.com).*
** *Electrical and Computer Engineering School, University of Campinas, Brazil*

Abstract: The autonomy of electric vehicles is under investigation by the scientific community, in which different solutions based on renewable energy resources, such as the photovoltaic, are proposed. A solution under study is the utilization of regenerative braking developed by the electric motor vehicles. In this work, the addition of a regenerative braking is proposed aiming to increase the autonomy of electric bicycles. A two level, three-phase converter is applied to drive a brushless DC motor (BLDC). A comprehensive modeling of current and speed control are presented in order to operate the machine in quadrants I and IV. The behavior of the Lithium battery charge is observed through its state-of-charge (SOC). Simulation results were obtained by means of the *SimPowerSystems®/ Matlab/Simulink®* software.

Keywords: Brushless DC motor, Current control, Speed control, Regenerative braking, Electric Bicycle.

1. INTRODUCTION

The electric propulsion vehicles are becoming a sustainable and economic alternative as a modern transportation system. This occurs not only because the environment sustainability appeal during global warming concern, but also because these vehicles are a rapid and economic means of transportation in urban area. Electric bicycles are included in this reality. On the other hand, the combustion vehicles inflict far more damage to the environment due to the emission of carbon dioxide, which speed up the global warming Ulrich (2005). Moreover, the usage of electric vehicle (EV) returns economic benefits, since the electric motors have an efficiency above 80 %, while a combustion motor has an average thermal efficiency of only 40 %. In addition, the electric motor maintenance is cheaper and simpler than the combustion motor Bertoluzzo and Buja (2011).

Regenerative braking can be used in electric bicycles as a process to regenerate the energy converted during the braking. During the regenerative braking, the energy is returned from the motor to the batteries, when the inertia of the bicycle forces the motor to enter in the generator mode Nian et al. (2014). At the same time, the electromagnetic braking torque is applied to reduce the velocity of the vehicle Wang et al. (2012).

Previous works have discussed the recovery of the braking energy Bahrami et al. (2019)Min et al. (2007). The regenerative braking process uses mainly the motor back electromotive force (EMF), which is used as an energy source to charge the battery. However, the EMF has to be sufficiently larger than the battery voltage in order to inject current for charging the battery. Usually, the EMF is lower than the battery voltage even during high speeds of operation, thus, many articles propose bidirectional dc-dc converters to boost up the EMF Wang et al. (1998). In Dixon and Ortuzar (2002), the dc-dc converter is coupled with supercapacitors that aid during the process of start and charge of the batteries, since during these processes the electric current grows fast, thereby reducing the batteries life span. Works as Nian et al. (2014); Yang et al. (2009); Naseri et al. (2016); Joy and Ushakumari (2018); Mohammad and Khan (2015) employ pulse generation techniques to change the gearshift of the EV during the process of regenerative braking.

This paper focuses on the mathematical modeling, compensation process of current and speed controllers, and the effect of the load disturbance in the control loop of a drive brushless DC motor employed in an electric bicycle. In addition, a process of regenerative braking is investigated. The regenerative braking is applied in order to convert the energy of the motor windings to boost up the dc link voltage, therefore injecting current to charge the battery.

2. BLDC MOTOR MODELING

The phase equations of a BLDC motor, taking into consideration the self and leakage inductances are expressed by:

$$V_{an} = R_a i_a + \frac{d}{dt}[L_{aa} i_a + L_{ba} i_b + L_{ca} i_c] + E_a \quad (1)$$

$$V_{bn} = R_b i_b + \frac{d}{dt}[L_{ab} i_a + L_{bb} i_b + L_{cb} i_c] + E_b \quad (2)$$

$$V_{cn} = R_c i_c + \frac{d}{dt}[L_{ac} i_a + L_{bc} i_b + L_{cc} i_c] + E_c \quad (3)$$

⋆ FAPESP grants

where V_{an}, V_{bn} and V_{cn} are the stator voltage phases; i_a, i_b and i_c are the stator electric current; R_a, R_b and R_c are the winding resistances; L_{aa}, L_{bb} are L_{cc} are self-inductances of the stator; L_{ba}, L_{ca}, L_{ab}, L_{cb}, L_{ac} and L_{bc} are the leakage inductances of each adjacent phase; and E_a, E_b and E_c are the back electromotive force of each phase.

Considering that the phase windings are equal, hence $R_a = R_b = R_c = R_s$ (where R_s is the general resistance of the stator); $L_{aa} = L_{bb} = L_{cc} = L$ (where L is the general self-inductance); $L_{ab} = L_{ac} = L_{ba} = L_{ca} = L_{cb} = M$ (where M is the general mutual inductance), whence one can obtain:

$$V_{an} = R_s i_a + \frac{d}{dt}[Li_a + Mi_b + Mi_c] + E_a \tag{4}$$

$$V_{bn} = R_s i_b + \frac{d}{dt}[Mi_a + Li_b + Mi_c] + E_b \tag{5}$$

$$V_{cn} = R_s i_c + \frac{d}{dt}[Mi_a + Mi_b + Li_c] + E_c \tag{6}$$

For a balanced system, then the currents $i_a + i_b + i_c = 0$; deriving the previous equation returns $\frac{di_a}{dt} + \frac{di_b}{dt} + \frac{di_c}{dt} = 0$, and: $-\frac{da}{dt} = \frac{db}{dt} + \frac{dc}{dt}$, $-\frac{db}{dt} = \frac{da}{dt} + \frac{dc}{dt}$, $-\frac{dc}{dt} = \frac{db}{dt} + \frac{da}{dt}$; replacing the derivatives in (4), (5), (6), respectively, yields:

$$V_{an} = R_s i_a + \frac{di_a}{dt}[L - M] + E_a \tag{7}$$

$$V_{bn} = R_s i_b + \frac{di_b}{dt}[L - M] + E_b \tag{8}$$

$$V_{cn} = R_s i_c + \frac{di_c}{dt}[L - M] + E_c \tag{9}$$

From (7),(8) and (9), it is possible to deduce the equivalent circuit of the BLDC motor, as shown in Fig. [1].

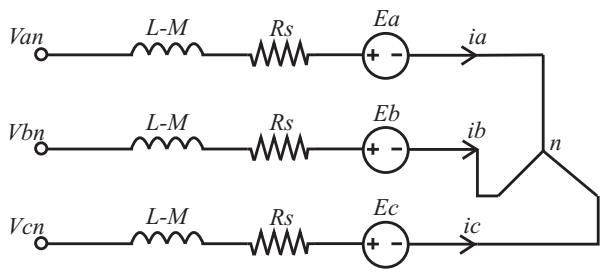

Figure 1. BLDC motor equivalent circuit.

The simplified stator equations can be obtained by doing $L_s = L - M$, thus:

$$V_{an} = R_s i_a + \frac{d}{dt} L_s i_a + E_a \tag{10}$$

$$V_{bn} = R_s i_b + \frac{d}{dt} L_s i_b + E_b \tag{11}$$

$$V_{cn} = R_s i_c + \frac{d}{dt} L_s i_c + E_c \tag{12}$$

The total electromagnetic torque developed by the phase currents is expressed by:

$$T_e = \frac{E_a i_a + E_b i_b + E_c i_c}{\omega_m} \tag{13}$$

The EMF induced in each phase is given as:

$$E_a = f_a(\theta_r)\lambda_p \omega_m \tag{14}$$

$$E_b = f_b(\theta_r)\lambda_p \omega_m \tag{15}$$

$$E_c = f_c(\theta_r)\lambda_p \omega_m \tag{16}$$

where λ_p is the flux constant and the functions $f_a(\theta_r)$, $f_b(\theta_r)$ and $f_c(\theta_r)$ represent the profile of E_a,E_b y E_c with magnitudes closed to ± 1, as expressed in (29).

By replacing (14), (15) and (16) in (13), the electromagnetic torque, in $N.m$, is written as:

$$T_e = \lambda_p[f_a(\theta_r)i_a + f_b(\theta_r)i_b + f_c(\theta_r)i_c] \tag{17}$$

The dynamic equation for a system with inertia J, friction coefficient B, and load torque T_l is given by:

$$J\frac{d\omega_m}{dt} + B\omega_m = (T_e - T_l) \tag{18}$$

whereat the rotor speed and position are related to each other by:

$$\frac{d\theta_r}{dt} = \frac{P}{2}\omega_m \tag{19}$$

where P is the number of poles, ω_m is the rotor speed in rad/s, and θ_r is the rotor position.

From the previous equations, the set of differential equations that represents the modeling of a BLDC motor is expressed by:

$$\frac{di_a}{dt} = -\frac{R_s i_a}{L} + \frac{V_a}{L} - \frac{\lambda_p f_a(\theta_r)\omega_m}{L} \tag{20}$$

$$\frac{di_b}{dt} = -\frac{R_s i_b}{L} + \frac{V_b}{L} - \frac{\lambda_p f_b(\theta_r)\omega_m}{L} \tag{21}$$

$$\frac{di_c}{dt} = -\frac{R_s i_c}{L} + \frac{V_c}{L} - \frac{\lambda_p f_c(\theta_r)\omega_m}{L} \tag{22}$$

$$\frac{d\omega_m}{dt} = -\frac{B\omega_m}{J} - \frac{T_l}{J} + \frac{\lambda_p f_a(\theta_r)i_a}{J} + \frac{\lambda_p f_b(\theta_r)i_b}{J} + \frac{\lambda_p f_c(\theta_r)i_c}{J} \tag{23}$$

$$\frac{d\theta_r}{dt} = \frac{P}{2}\omega_m \tag{24}$$

From (20), (21), (22), (23), (24), the model state equations yields $\dot{X}^T = \left[\dot{i_a}(t)\ \dot{i_b}(t)\ \dot{i_c}(t)\ \dot{\omega_m}(t)\ \dot{\theta_r}(t)\right]$, and:

$$\dot{X} = \begin{bmatrix} -\frac{R_s}{L} & 0 & 0 & \frac{\lambda_p f_a(\theta_r)}{L} & 0 \\ 0 & -\frac{R_s}{L} & 0 & \frac{\lambda_p f_b(\theta_r)}{L} & 0 \\ 0 & 0 & -\frac{R_s}{L} & \frac{\lambda_p f_c(\theta_r)}{L} & 0 \\ \frac{\lambda_p f_a(\theta_r)}{J} & \frac{\lambda_p f_b(\theta_r)}{J} & \frac{\lambda_p f_c(\theta_r)}{J} & -\frac{B}{J} & 0 \\ 0 & 0 & 0 & \frac{P}{2} & 0 \end{bmatrix}$$

$$\begin{bmatrix} i_a(t) \\ i_b(t) \\ i_c(t) \\ \omega_m(t) \\ \theta_r(t) \end{bmatrix} + \begin{bmatrix} \frac{1}{L} & 0 & 0 & 0 \\ 0 & \frac{1}{L} & 0 & 0 \\ 0 & 0 & \frac{1}{L} & 0 \\ 0 & 0 & 0 & \frac{-1}{J} \end{bmatrix} \begin{bmatrix} V_a(t) \\ V_b(t) \\ V_c(t) \\ T_l \end{bmatrix} \tag{25}$$

which can be expressed in a vector form as:

$$\frac{\boldsymbol{di(t)}}{dt} = -\frac{R_s \boldsymbol{i(t)}}{L} + \frac{\boldsymbol{v(t)}}{L} - \frac{\lambda_p \boldsymbol{f(\theta_r)} \omega_m}{L} \tag{26}$$

$$\frac{d\omega_m}{dt} = -\frac{B\omega_m}{J} - \frac{T_l}{J} + \frac{\lambda_p \boldsymbol{f(\theta_r)i(t)}}{J} \tag{27}$$

$$\frac{d\theta_r}{dt} = \frac{P}{2}\omega_m \tag{28}$$

The profiles of the ideal EMF for the three phases are shifted from one another by 120°. The function that represents the a phase is:

$$f(\theta_r) = \begin{cases} 1, & 0 \geq \theta_r < \frac{2\pi}{3} \\ 1 - \frac{6(\theta_e - \frac{2\pi}{3})}{\pi}, & \frac{2\pi}{3} \geq \theta_r < \pi \\ -1, & \pi \geq \theta_r < \frac{5\pi}{3} \\ -1 + \frac{6(\theta_e - \frac{5\pi}{3})}{\pi}, & \frac{5\pi}{3} \geq \theta_r < 2\pi \end{cases} \tag{29}$$

Finally, for each b and c phase, (29) is shifted by $2\pi/3$ and $4\pi/3$ rads, respectively.

3. BLDC MACHINE CONTROL

By controlling the BLDC motor using a two level, three-phase converter, two phases are always conducting current. In this way, the currents are in opposite directions, which can be expressed by:

$$i_a = -i_b = i; \quad \frac{di_a}{dt} = -\frac{di_b}{dt} = \frac{di}{dt} \tag{30}$$

Thus, the line-to-line voltage u_{AB} can be expressed by replacing (30) in (7) and (8), such as:

$$u_{AB} = 2R_s + 2(L - M)\frac{di}{dt} + (E_a - E_b) \tag{31}$$

Considering that no commutation occurs in the transient part of the EMF, then the stationary part E_a and E_b are equal in amplitude and in opposite directions, when the phases A and B are operating. Hence, (31) can be expressed as:

$$u_{AB} = 2R_s + 2L\frac{di}{dt} + 2E_a = R_a i + L_a \frac{di}{dt} + ke\omega \tag{32}$$

From the previous expression, the equivalent circuit is shown in Fig. 2, in which R_a, L_a are the equivalent resistance and inductance expressed in similar fashion as the DC motor with brushes.

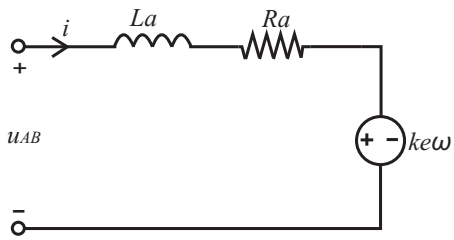

Figure 2. Equivalent circuit of the BLDC motor with two exciting phases.

Before applying the Laplace transform, it is possible to verify that (26),(27),(28) are linear. Thus, the constant $ke = 2P\lambda_p$ is defined from (32) and $kt = 2P\lambda_p$ is defined from the torque equation of two conducting phases. By applying such constants, replacing (32) in (26) and (27); (28) becomes linear as:

$$\frac{di(t)}{dt} = -\frac{R_a i(t)}{L_a} + \frac{u_{AB}}{L_a} - \frac{k_e \omega_m}{L_a} \tag{33}$$

$$\frac{d\omega_m}{dt} = -\frac{B\omega_m}{J} - \frac{T_l}{J} + \frac{k_t i(t)}{J} \tag{34}$$

$$\frac{d\theta_r}{dt} = \frac{P}{2}\omega_m \tag{35}$$

By applying the Laplace transform into (33), (34), and (35), one has:

$$i(s)(L_a s + R_a) = \underbrace{-ke\omega(s) + u_{AB}}_{V_L(s)} \tag{36}$$

$$\omega(s)(Js + B) = \underbrace{kti(s) - T_l}_{a(s)} \tag{37}$$

where the state variable $V_L(s)$ is the winding voltage and $a(s)$ is the rotor acceleration.

Equations (36) and (37) are represented by a signal-flow graph as:

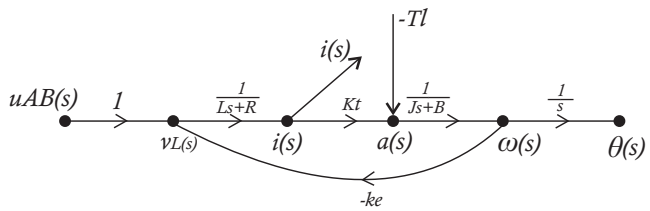

Figure 3. Signal-flow graph of the control system.

In the signal-flow graph shown in Fig. 3, it is observed the state variables have as inputs the phase voltage $u_{AB}(s)$ and the load torque T_l, and as outputs $i(s)$ and $\theta(s)$. The power converter is modeled as a first-order transfer function $Gc(s) = \frac{k_r}{1 + sT_r}$, with gain $k_r = 0.65\frac{V_{dc}}{V_{cm}}$; where V_{dc} is the dc-bus voltage; V_{cm} is the maximum control voltage of the modulator. In addition, $T_r = \frac{1}{2f_c}$, where f_c is the converter switching frequency Krishnan (2017).

With the modeling of the power converter, it is possible to close the inner current control and the outer speed control loops, with unit feedback gain, by neglecting the feedback

gains in the signal-flux graph in Fig. 3. In Fig. 4, the signal-flux graph is shown for the current and speed control, in which the input is the speed reference $\omega_{ref}(s)$.

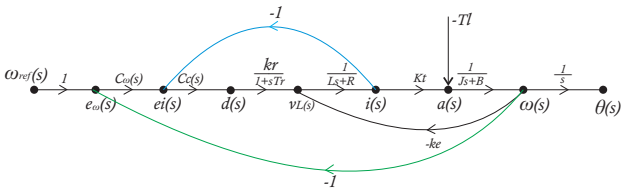

Figure 4. Signal-flux graph of current and speed control.

3.1 BLDC machine current control

The current transfer function is obtained from the signal-flux graph (Fig. 4) by using the Mason equation:

$$Giu(s) = \frac{i(s)}{u_{AB}(s)}|_{T_l=0} = \frac{Js+B}{(Ls+R_s)(Js+B)+K_tK_e} \tag{38}$$

In the signal-flux graph shown in Fig. 3, it is observed that the system has two inputs. By applying the homogeneity principle, the transfer function of the current control is obtained (Fig. 3). It is worth noting that the torque disturbances are considered as low frequency ones; which are mitigated by the current controller due to its fast and high gain characteristics at low frequencies.

Aiming to increase the cutoff frequency, speed, and phase margin of the current control loop, also aiming to reduce the maximum overshoot, a lead compensator is added together with an integrator previously designed to achieve $e_{ss} = 0$. The adopted cutoff frequency and phase margin are $Fc = 500\ rad/s$ and $MF = 70°$, respectively. The Bode Graph is depicted in Fig. 5.

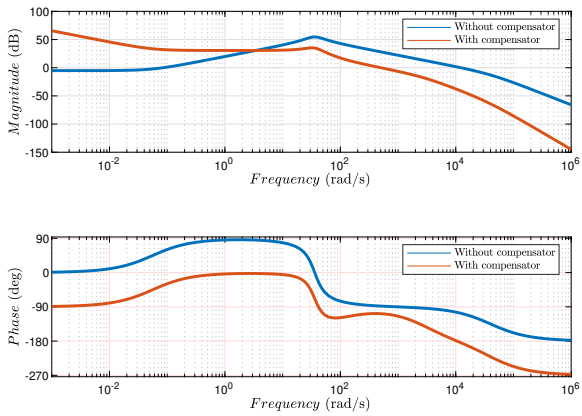

Figure 5. Frequency response of the current compensator.

The capacity of the current control loop for rejecting load torque disturbance is analyzed starting from the relation:

$$\frac{i(s)}{T_l(s)} = \frac{G_{iT_l}}{1+T(s)} \tag{39}$$

where G_{iT_l} is the transfer function that relates $i(s)$ with $T_l(s)$, $T(s) = C_c(s)Gc(s)Giu(s)H_i(s)$ is the loop gain, wherein $C_c(s)$ is the current compensator and $H_i(s)$ is the feedback gain.

Load torque disturbance is an unknown parameter with respect to the time variable, which hinders the machine efficiency performance during the interval of operation Li et al. (2012). Fig. 6 shows that the rejection capacity of the load torque in the current control loop is approximately -30 dB. By increasing the controller gain, it is possible to improve the rejection capacity of the load torque at low frequencies.

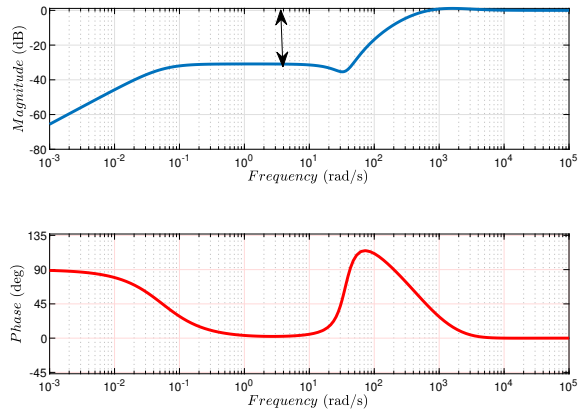

Figure 6. Disturbance rejection capacity.

3.2 BLDC machine speed control

The signal-flux graph used to obtain the speed control loop is shown in Fig. 7. This graph shows two inputs and one output, in which $i_{ref}(s)$ is the input, wherein the speed control operates. Therefore, it is necessary to have knowledge of the transfer function $\frac{\omega(s)}{i_{ref}(s)}$.

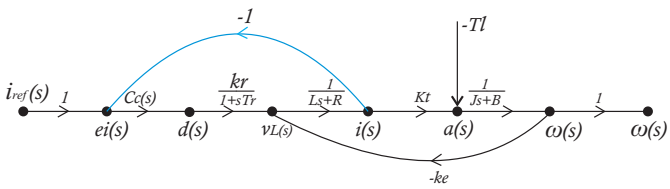

Figure 7. Signal-flux graph of $\frac{\omega(s)}{i_{ref}(s)}$.

The other input is T_l, which is considered as a disturbance input that acts over the electromagnetic torque produced by the BLDC machine. This disturbance input has low frequency and time-variant characteristics, thereby being attenuated by the compensator. In order to achieve the compensation goal, Mason method is applied to the transfer function, which yields:

$$\frac{\omega(s)}{i_{ref}(s)}|_{T_l=0} = \frac{Cc(s)k_rk_e}{((L_as+R_a)(1+T_rs)+k_rCc(s))(Js+B)+k_tk_e(1+T_rs)} \tag{40}$$

Fig. 8 shows the Bode Graph of the open loop, compensated, speed control system. Similarly with the current control loop, the compensator consists of an integrator, ensuring a ramp response; and also a lead compensator to increase the phase margin and the system time response.

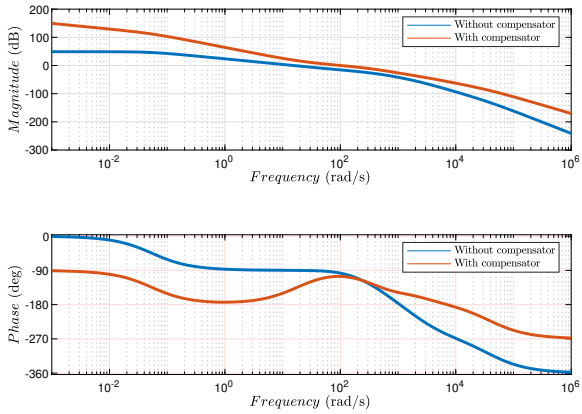

Figure 8. Frequency response of the speed transfer function compensation.

4. SIMULATION AND RESULTS

This section shows the results of the current and speed cascade control loops, as well as the regenerative braking operating at the first and fourth quadrants. The simulations presented in this section are based on the parameters in Tab. 1.

Table 1. BLDC motor parameters

BLDC motor	Value	Unit
Stator Resistance	0.2	Ω
Stator inductance	8.5e-3	H
Inertia moment	0.089	kg.m.m
Viscous friction coefficient	0.005	N.m.s
Pole numbers	4	-
Torque constant	1.4	N.m

4.1 Motor operation mode

Fig. 9 shows the speed control without load on the shaft, in which a ramp profile is imposed as the speed reference. From Fig. 9, it is possible to see that the current control tracks the rectangular references, which are a characteristic of the BLDC motor. In Fig. 9.b, the ramp references of the speed control is shown. It is verified that the speed control follows the imposed reference. Moreover, Fig. 9.c shows that the electromagnetic torque references are satisfactorily tracked, imposing acceleration and deceleration according to the speed profile command.

4.2 Regenerative braking operation mode

The regenerative braking is achieved by inverting the direction of the current in the circuit formed by the battery and the motor. In such circuit, the EMF operates as a voltage source, which is lower the battery voltage (at low speeds of operation). To achieve this goal, the same two level, three-phase converter can be employed if appropriate commutation is implemented Marchesoni and Vacca (2007). In this work, the braking mode is achieved by decelerating the speed profile in a way that the torque sense is inverted, thus imposing the braking due to the vehicle inertia.

In Fig. 10, three graphics are shown representing the speed of the electric bicycle, the electromagnetic torque and the

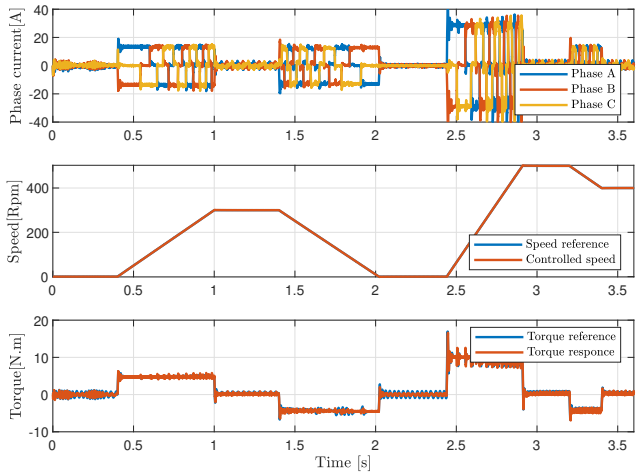

Figure 9. Current and speed control responses.

battery state-of-charge. Considering that the electric bicycle is in a downhill slope and $T_l = -5N.m$, it is observed that the BLDC motor operates in the fourth quadrant, with positive speed and negative electromagnetic torque.

Initially, between $[0s - 0.4s]$, the electric bicycle is stopped. However, the electromagnetic torque is negative because the torque $T_l = -5$ N.m favors the imposed movement. Thus, to keep the bicycle with zero speed, the controller imposes the negative torque such as:

$$T_e - (T_l) => T_e - (-5N.m) = J\frac{d\omega}{dt} = 0 => T_e = -5N.m \tag{41}$$

In the interval $[0.4s - 1s]$, the speed of the electric bicycle is gradually increased from 0 to 300 r/min. In this interval, the electromagnetic torque presents a small braking, thereby generating energy, as can be seen by the lithium battery SOC. In the interval $[1s - 1.4s]$, the speed is constant at 300 r/min, which returns a null derivative ($\frac{d\omega}{dt} = 0$). Hence, the electromagnetic torque has the same magnitude as the load torque ($T_e = -5$ N.m), as shown in (41). In addition, due to this fact, the SOC slope is increasing, which indicates that the battery is being charged.

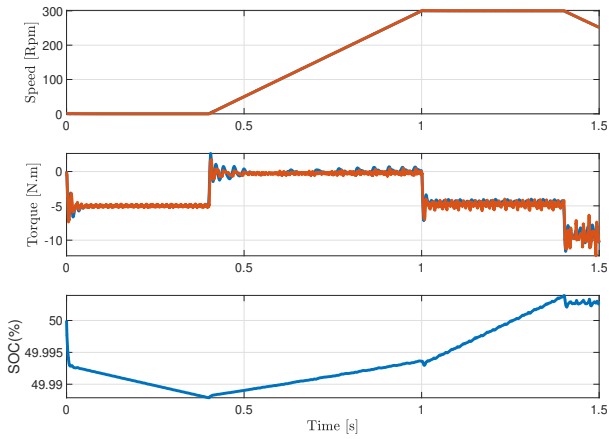

Figure 10. Electric bicycle operation at the fourth quadrant

Continuing the assumption that the electric bicycle is in a downhill slope, the operation at the first and fourth quadrants are depicted in Fig.11. In the interval $[2.5s - 2.9s]$, the BLDC motor operates at the first quadrant (conduction mode) with positive electromagnetic torque. Due to the conduction mode, the battery provides energy to the motor, as can be seen by the positive electric power and a decreasing SOC, which indicates energy consumption. In the interval $[2.9s - 3.7s]$, the BLDC machine operates in the regenerative braking mode. The power is negative and the SOC increases, which indicates that the dc-link current direction was inverted and the battery is being charged.

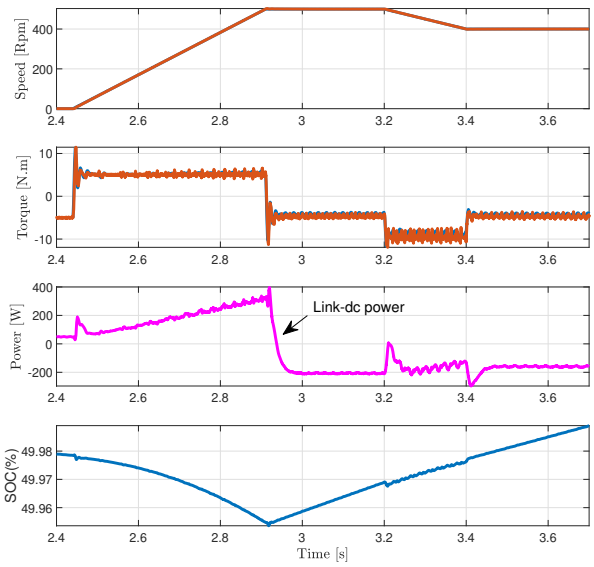

Figure 11. Electric bicycle operation at the first and fourth quadrant

5. CONCLUSION

This work presents the mathematical modeling and control design of a BLDC motor applied in electric bicycles vehicles. The characteristics of current and speed compensators are emphasized, as well as the capacity of the controllers to reject disturbances. The response of the designed current controller is effective, wherein an integrator and a lead compensator are cascaded together to increase the capacity of rejecting load torque disturbances at low frequencies. On the other hand, the speed control tracked satisfactorily the speed ramp reference, which is characteristic of an acceleration and deceleration of electric vehicles. In addition, the recovery of the energy dissipated when the bicycle faces a downhill slope was analyzed. The results show the effectiveness of the regenerative braking during the deceleration, in which the energy is converted back to charge the lithium battery, as highlighted by its state-of-charge analysis and by the inversion of the dc-link current direction.

ACKNOWLEDGMENTS

The authors would like to thanks CAPES for providing scholarship.

REFERENCES

Bahrami, M., Mokhtari, H., and Dindar, A. (2019). Energy regeneration technique for electric vehicles driven by a brushless dc motor. *IET Power Electronics*, 12(13), 3397–3402.

Bertoluzzo, M. and Buja, G. (2011). Development of electric propulsion systems for light electric vehicles. *IEEE Transactions on Industrial Informatics*, 7(3), 428–435.

Dixon, J.W. and Ortuzar, M.E. (2002). Ultracapacitors+ dc-dc converters in regenerative braking system. *IEEE Aerospace and Electronic Systems Magazine*, 17(8), 16–21.

Joy, J. and Ushakumari, S. (2018). Regenerative braking mode operation of a three-phase h-bridge inverter fed pmbldc motor generator drive in an electric bike. *Electric Power Components and Systems*, 46(19-20), 2174–2188.

Krishnan, R. (2017). *Permanent magnet synchronous and brushless DC motor drives*. CRC press.

Li, S., Xia, C., and Zhou, X. (2012). Disturbance rejection control method for permanent magnet synchronous motor speed-regulation system. *Mechatronics*, 22(6), 706–714.

Marchesoni, M. and Vacca, C. (2007). New dc–dc converter for energy storage system interfacing in fuel cell hybrid electric vehicles. *IEEE Transactions on Power Electronics*, 22(1), 301–308.

Min, Y., Zhifeng, B., and Binggang, C. (2007). Robust h 2/h infinity control for regenerative braking of electric vehicles. In *2007 IEEE International Conference on Control and Automation*, 1366–1370. IEEE.

Mohammad, A. and Khan, M.Z.R. (2015). Bldc motor controller for regenerative braking. In *2015 International Conference on Electrical Engineering and Information Communication Technology (ICEEICT)*, 1–6. IEEE.

Naseri, F., Farjah, E., and Ghanbari, T. (2016). An efficient regenerative braking system based on battery/supercapacitor for electric, hybrid, and plug-in hybrid electric vehicles with bldc motor. *IEEE Transactions on Vehicular Technology*, 66(5), 3724–3738.

Nian, X., Peng, F., and Zhang, H. (2014). Regenerative braking system of electric vehicle driven by brushless dc motor. *IEEE Transactions on Industrial Electronics*, 61(10), 5798–5808.

Ulrich, K.T. (2005). Estimating the technology frontier for personal electric vehicles. *Transportation research part C: Emerging technologies*, 13(5-6), 448–462.

Wang, F., Yin, X., Luo, H., and Huang, Y. (2012). A series regenerative braking control strategy based on hybrid-power. In *2012 International Conference on Computer Distributed Control and Intelligent Environmental Monitoring*, 65–69. IEEE.

Wang, K., Lin, C.Y., Zhu, L., Qu, D., Lee, F.C., and Lai, J.S. (1998). Bi-directional dc to dc converters for fuel cell systems. In *Power Electronics in Transportation (Cat. No. 98TH8349)*, 47–51. IEEE.

Yang, M.J., Jhou, H.L., Ma, B.Y., and Shyu, K.K. (2009). A cost-effective method of electric brake with energy regeneration for electric vehicles. *IEEE Transactions on Industrial Electronics*, 56(6), 2203–2212.